Journal of Power Sources 241 (2013) 567–571

Contents lists available at SciVerse ScienceDirect

Journal of Power Sources

journal homepage: www.elsevier.com/locate/jpowsour

Short communication

On the growth of nanostructured iron hydroxy-fluorides for Li-ion batteries

B. Guitián [a], S. Lascaud [b], X.R. Nóvoa [a,*], L. Ribeaucourt [b], E. Vidal [b]

[a] ENCOMAT Group, Universidade de Vigo, EEI, Campus Universitario, 36310 Vigo, Spain
[b] EDF R&D, Av. des Renardières, Ecuelles, 77818 Moret-sur-Loing cedex, France

HIGHLIGHTS

- Electrochemically grown nano-structured hydroxyl fluorides.
- Impedance-based methodology for in-situ characterization.
- Conversion reaction for material preparation and energy recovering.

GRAPHICAL ABSTRACT

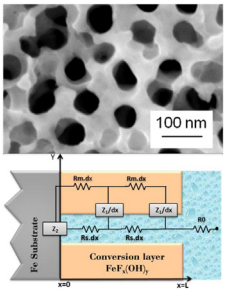

ARTICLE INFO

Article history:
Received 20 October 2012
Received in revised form
24 April 2013
Accepted 28 April 2013
Available online 15 May 2013

Keywords:
Conversion reaction
Cathode material
Rechargeable lithium batteries
Iron hydroxyfluoride

ABSTRACT

Lithium ion battery applications such as transportation or renewable energies require cost effective, environmentally friendly and high capacity materials. Conversion reaction with iron based materials at positive electrode is a promising route to reach this target.

In this work, iron hydroxyl-fluoride conversion coatings are prepared by an electrochemical way. The structure of the produced coatings is nano-porous with a pore diameter of about 75 nm. An impedance-based methodology is proposed for in-situ characterisation of the conversion coatings during the preparation procedure and enables to optimize the process parameters to get a 3D nano-porous structure. The cycling tests performed in coin-cell versus lithium reference electrode show a promising cycling behaviour for the prepared nano-porous coatings.

1. Introduction

In order to improve the technical and economical performance of energy storage, most of the research in this field is focused on the development of new electrode materials for batteries. Particularly, lithium-ion batteries have important capacity limitations due to the electrode materials mainly at the positive electrode. An alternative proposed to increase the capacity could be the use of nanostructured materials, such as nanostructured iron fluorides for positive electrode. These materials enable to obtain high specific capacity [1,2] on the order of 700 mAh g^{-1}.

Most papers dedicated to the study of electrode materials are based on the use of powders whose characterization is done a posteriori, on the compacted sample, by X-ray diffraction, XRD, and Scanning electron Microscopy, SEM, examination and composite electrodes (including the powders mixed with a binder and a conducting agent spread on a metallic sheet) are made to evaluate the electrochemical properties as battery material. Nevertheless, the approach reported in the present paper is

* Corresponding author. Tel.: +34 986812213.
E-mail addresses: rnovoa@uvigo.es, xramonnovoa@gmail.com (X.R. Nóvoa).

0378-7753/$ – see front matter © 2013 Elsevier B.V. All rights reserved.
http://dx.doi.org/10.1016/j.jpowsour.2013.04.145

different because conversion layers constituting the active material of the electrode are directly developed on the electrode, which makes it bi-functional: holder of the active material and current collector.

This new approach requires a tool capable of providing information on the development of the layer during the growth period. The Electrochemical Impedance Spectroscopy, EIS, was chosen for this purpose and first results are the subject of this communication.

2. Experimental

2.1. Preparation and in-situ characterisation of the conversion coatings

The substrate material used was an iron strip (Goodfellow, 99.99%) constituting the working electrode of an electrochemical cell with a platinum mesh as counter electrode and a Pt wire as pseudo reference electrode. The nominal active surface areas of the working electrodes were between 0.28 cm^2 and 2.0 cm^2, depending on the further test requirements.

The formation of conversion coatings was carried out by anodizing in a range of applied potential (two electrodes) between 25 V and 150 V, for up to 15 min. The best results in terms of porosity were obtained at 50 V for 15 min and are the object of the present report. The electrolyte solutions used were based on ethylene glycol (ETG) and water [3] containing NH_4F.

The expected electrochemical processes are:

a) At the anode (the iron working electrode):
- Formation of the conversion layer through the process

$$Fe + xF^- \rightarrow FeF_x^{(3-x)+} + 3e^-$$

- Water oxidation through the process

$$H_2O \rightarrow \frac{1}{2}O_2 + 2H^+ + 2e^-$$

b) At the cathode (the platinum counter electrode):
- Reduction of the ammonium cations through the process

$$NH_4^+ + e^- \rightarrow NH_3 + \frac{1}{2}H_2$$

- Water reduction through the process

$$2H_2O + 2e^- \rightarrow 2OH^- + O_2$$

Thus, a fluoride-rich conversion layer will be produced together with a side reaction which is water electrolysis.

The characterization of the coatings by EIS was done in the same solution after interrupting the electrolysis current and stabilization of the potential. The impedance was then determined at the open circuit potential using Pt pseudo reference, between 10 kHz and 10 mHz, taking seven points per decade and using an AC amplitude of 10 mV rms. The measures were managed by a system AUTOLAB (Ecochemie®) based on a potentiostat PGSTAT 30.

2.2. Cycling and ex-situ characterisation of the conversion coatings

Square shaped samples of 1 cm^2 were dried at 80 °C under vacuum for 2 h. A 2035-size coin cell was made to examine the electrochemical properties of the layer. The cell was assembled in a glove box filled with dry air. Lithium foils (Chemetall Foote Corp.) and polypropylene films were used as counter electrode and separator, respectively. The electrolyte used was 1 M $LiPF_6$ dissolved in ethylene carbonate, EC/diethyl carbonate, DEC, solution (1/1, v/v). The coin cells were galvanostatically cycled using a 30 μA cm^{-2} current density and a voltage window of 1.5 V–4 V.

The morphology of the fluoride layer was investigated by scanning electron microscopy (FEG-SEM Zeiss Supra 55) before cycling and after 200 charge–discharge cycles. To do so, the coin cell was stopped after 200 cycles at 4 V in the charged state. Then, it was dis-assembled in the glove-box, rinsed in a dimethyl carbonate (DMC) solution and dried in the glove box before SEM observation.

3. Results and discussion

3.1. Preparation and in-situ characterisation of the conversion coatings

The general trend of the chronoamperograms obtained during the electrolysis is depicted in Fig. 1A. The presence of three domains is easily distinguished: Germination (0–30 s), growth (30–120 s) and a pseudo steady state from 120 s.

The exponential decay of the current observed in Fig. 1A can be attributed to the fast formation of a passive layer, as evidenced by the high impedance values obtained, as shown in Fig. 1B for 5 s and 20 s of electrolysis. After that initial short period, the current

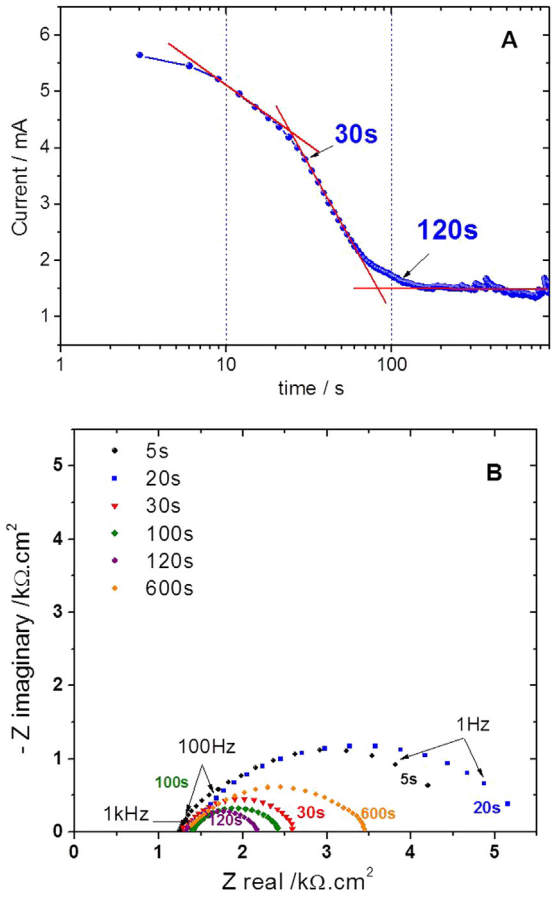

Fig. 1. A) Chronoamperogram obtained during the synthesis of a conversion layer on a 0.20 cm^2 Fe electrode at 50 V in ETG solution containing NH_4 F and H_2O. B) Nyquist impedance diagrams recorded at selected times during the electrolysis.

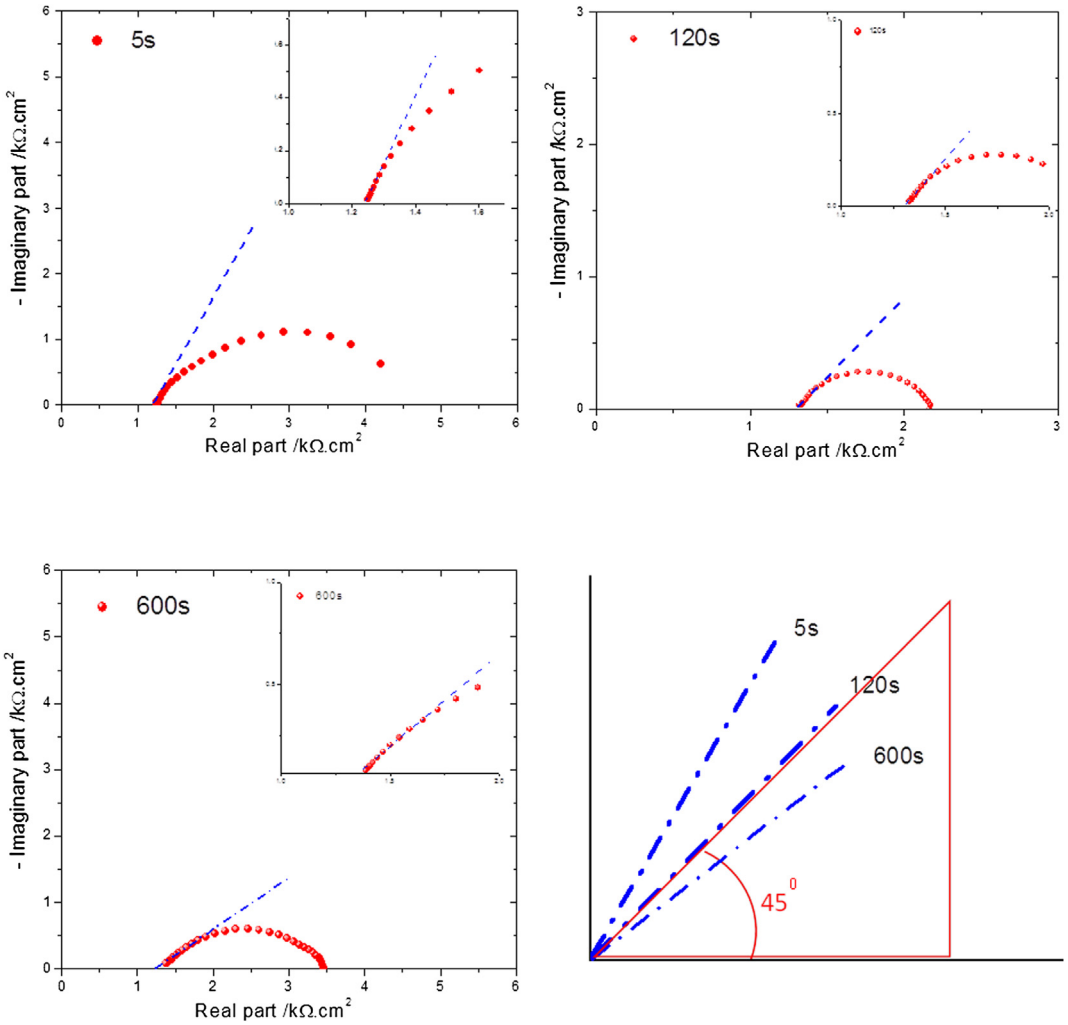

Fig. 2. Illustration of the evolution of the phase angle of the impedances obtained in-situ with the time of electrolysis (5 s, 120 s and 600 s).

keeps on decreasing till about 120 s, and the impedance of the interface follows the same trend, which can be attributed to a development of the passive layer in 3D, leading to increasing roughness. This hypothesis can be verified in the closer look to the high frequency limit of impedance spectra, summarised in Fig. 2.

The evolution of the phase angle shown in Fig. 2 is consistent with the transition from a planar electrode morphology to a porous one of with conductive walls, according to the de Levie model [4].

3.2. Ex-situ characterisation of the conversion coatings

SEM examination of the electrolysed surfaces shows a well-developed porous nano-structure, as depicted in Fig. 3A. The chemical composition, from EDX analysis, is given in Fig. 3B. The formation of an iron oxy-(or hydroxy)-fluoride is confirmed.

From Fig. 3 the density of pores can be estimated at about 10^{10} pores cm^{-2}, and the average pore diameter at 75 nm. Assuming cylindrical geometry, those values allow estimating 44% open porosity (4.4×10^{-11} cm^2 as pore section) for the coating.

Mechanical profilometry (Veeco's Dektak® 150 Surface Profiler) allowed estimating the thickness of the conversion coating at 10 μm.

Knowing the thickness and the porosity of the coating, 1.5 mg cm^{-2} can be estimated as active mass with respect to the surface area.

3.3. Modelling of the EIS data

As discussed in Section 3.1, the structure of the conversion layer seems to evolve rapidly from 2D morphology to a 3D structure, confirmed by the SEM examination presented in the previous section (*cf.* Fig. 3A). The structure and the electrical properties of the developed coating are aspects of major interest both for the optimisation of the preparation process and for the further performance of the battery electrode material. In this context, electrical analogues are very useful tools for modelling the electrochemical systems. In view of the data presented in Sections 3.1 and 3.2, an appropriate electrical analogue to use in the present case to characterise the pore structure is that developed by Macdonald for porous magnetite-based layers on steel [5]. Variations of this model have been successfully used to study other types of conducting coatings [6].

Fig. 4A depicts an example of the experimental impedance data corresponding to the steady state development of the porous structure and the fitted data using Equation (1) as the impedance model corresponding to the equivalent electrical analogue depicted in Fig. 4B. A good agreement can be observed between the experimental and fitted data.

$$Z(\omega) = R_0 + \frac{R_m \cdot R_s}{Z_m + R_m} L + \frac{\sqrt{\gamma}\left(2R_m R_s + \left(R_m^2 + R_s^2\right)\cosh\left(L\sqrt{\gamma}\right)\right) + \delta R_s^2 \sinh\left(L\sqrt{\gamma}\right)}{\sqrt{\gamma}(R_m + R_s)\left(\sqrt{\gamma}\sinh\left(L\sqrt{\gamma}\right) + \delta\cosh\left(L\sqrt{\gamma}\right)\right)}$$

$$\text{with } \gamma = \frac{R_m + R_s}{Z_1(\omega)} \text{ and } \delta = \frac{R_m + R_s}{Z_2(\omega)}, \text{ being } Z_i(\omega) = \frac{R_i}{1 + (j\omega R_i C_i)^{\alpha_i}} \ (i = 1, 2) \quad (1)$$

The impedance data were analysed using the "downhill simplex method" developed by Nelder and Mead [7]. The function to minimise, χ^2, is defined in Equation (2) where N is the total number of scanned frequencies, a_{ei} and b_{ei} are respectively the real and imaginary parts of the experimental impedance, Z_{ei}, at frequency i, and a_{ci} and b_{ci} the corresponding real and imaginary parts of the calculated impedance at frequency i.

$$\chi^2 = \sum_{i=1}^{N}\left[\left(\frac{a_{ei} - a_{ci}}{|Z_{ei}|}\right)^2 + \left(\frac{b_{ei} - b_{ci}}{|Z_{ei}|}\right)^2\right] \quad (2)$$

In Equation (1) and Fig. 4B, R_m corresponds to the resistance per unit of length of the oxy-fluoride phase. R_m corresponds to the resistance per unit of length of the electrolyte inside the pores. Z_1 is the interfacial impedance at pore walls, taken here as a simple charge transfer resistance and double layer capacitance with a Cole–Cole type dispersion represented by α_1. Z_2 corresponds to the impedance at the pore's bottom, taken also as a simple charge transfer resistance and double layer capacitance with a Cole–Cole type dispersion represented by α_2. R_0 holds for the electrolyte resistance between the reference electrode and the pore opening.

In Table 1 it is worth to note that the R_s value well corresponds to the electrolyte resistivity, 617 Ω cm normalised to the geometry and distribution of pores discussed in Section 3.2, according to Equation (3).

$$R_s(\Omega\,\text{cm}) = \frac{R_{\text{pore}}(\Omega)}{N_{\text{pore}}(\text{cm}^{-2}) \cdot L_{\text{pore}}(\text{cm})} = \frac{\rho_{\text{electrolyte}} \cdot L_{\text{pore}}/S_{\text{pore}}}{N_{\text{pore}} \cdot L_{\text{pore}}} = \frac{\rho_{\text{electrolyte}}}{N_{\text{pore}} \cdot S_{\text{pore}}} = \frac{617}{10^{-10} \times 4.4 \cdot 10^{-11}} = 1.4\,\text{k}\Omega\,\text{cm} \quad (3)$$

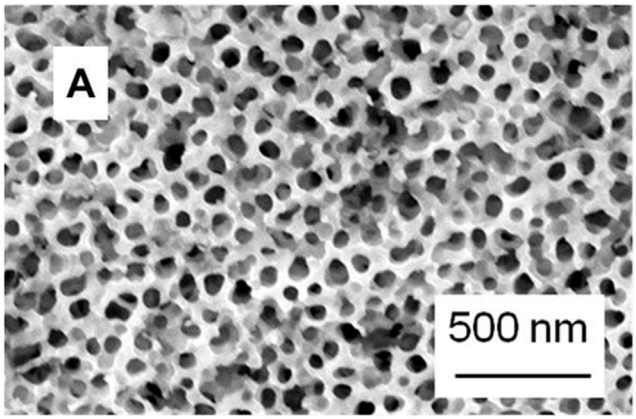

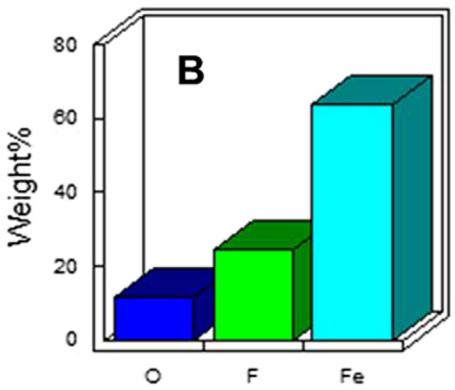

Fig. 3. A) SEM image of the conversion layer formed at 50 V for 15 min. B) EDX analysis of the conversion layer showing its oxy-fluoride nature.

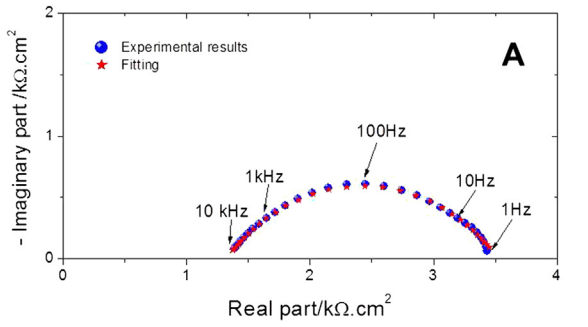

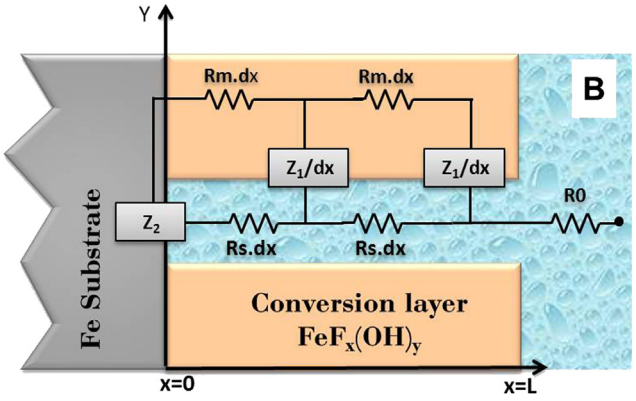

Fig. 4. A) Experimental impedance data obtained at 600 s (Fig. 1) and fitted data using Equation (1) as model impedance. B) Illustration of the equivalent electrical model.

Table 1
Best fitting parameters obtained for the fitting of data in Fig. 4 to the impedance given in Equation (1). $\chi^2 = 0.44$.

R_0 Ω cm²	R_m Ω cm	R_s Ω cm	R_1 Ω cm³	C_1 μF cm⁻³	α_1	R_2 Ω cm²	C_2 μF cm⁻²	α_2	L cm
1320	1.3E7	1.3E3	3.4	224	1	3227	0.77	0.6033	0.001

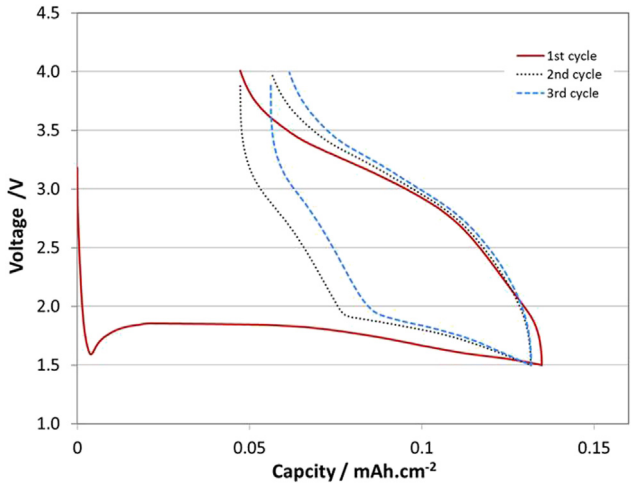

Fig. 5. Discharge and charge curves of a lithium cell with $FeF_x(OH)_y$ conversion layer grown on pure iron substrate after 15 min at 50 V, with 1 M $LiPF_6$ EC/DEC electrolyte at 25 °C.

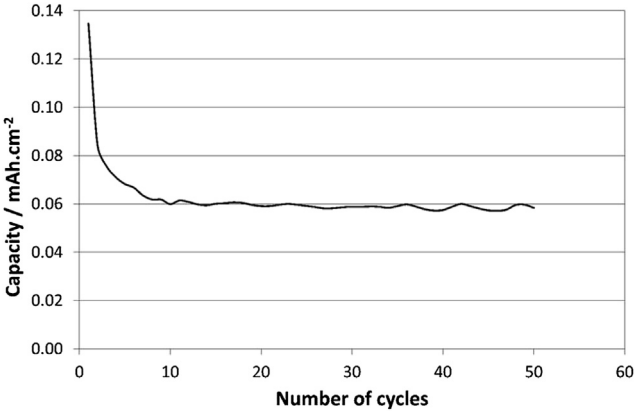

Fig. 6. Discharge capacity plotted as a function of the cycle number for a lithium cell with $FeF_x(OH)_y$ conversion layer grown on pure iron substrate.

The comparison of R_s and R_m values allows an estimation of the resistivity of the conversion layer that occupies 56% the surface of the electrode. Thus, the resistivity of the bulk hydroxyfluoride coating is about 10^4 that of the bulk electrolyte, in agreement with the dielectric character of iron fluorides.

3.4. Cycling in coin cell

The charge discharge profile of the hydroxyl fluoride electrode is shown in Fig. 5. A voltage plateau consistent with a conversion reaction is observed at 1.85 V. It is in agreement with what is observed in the literature [1,8]. The first discharged capacity corresponds to 0.13 mAh cm^{-2} or 80 mAh g^{-1} of extracted capacity (for 1.5 mg cm^{-2} of hydroxy-fluoride), which is rather low as compared

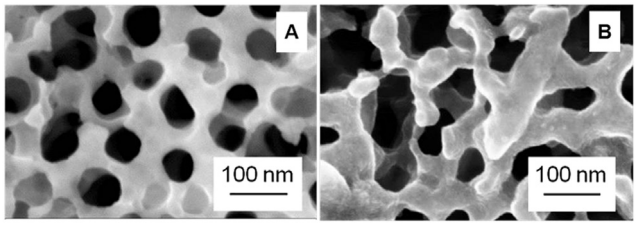

Fig. 7. SEM images of the $FeF_x(OH)_y$ conversion layers formed at 50 V. A) Before cycling. B) After 200 cycles.

to the theoretical capacity (571 mAh g^{-1} for FeF_2 and 712 mAh g^{-1} for FeF_3). The reaction is only partially reversible: 36% loss of capacity is observed at the second cycle.

As displayed in Fig. 6, the discharged capacity stabilizes at 0.06 mAh cm^{-2}, which is 46% of the initial capacity. Good capacity retention is observed upon cycling afterwards.

Fig. 7 shows SEM images of the $FeF_x(OH)_y$ conversion layers formed after 15 min at 50 V before cycling (a) and after 200 cycles (b). The nanotubular structure of the layer is still present after 200 cycles but with more holes and higher porosity. This is an encouraging result.

4. Conclusions

Iron hydroxyfluoride conversion coatings were prepared by an electrochemical way. The coatings produced have a nano-porous structure with a pore diameter of about 75 nm. A method based on EIS is proposed for the in-situ characterisation of the electrochemical properties of the conversion coating that allows fine tuning of the synthesis parameters.

That structure provides good cycling behaviour in coin-cell arrangement, although the capacitance recovered is rather poor in the conditions of the test.

Acknowledgements

The Spanish authors would like to thank the Spanish Government for partially funding this work under project #BIA2010-16950.

References

[1] N. Pereira, F. Badway, M. Wartelsky, S. Gunn, G.G. Amatucci, J. Electrochem. Soc. 156 (2009) A407.
[2] H. Arai, S. Okada, Y. Sakurai, J. Yamaki, J. Power Sources 68 (1997) 716.
[3] R.R. Rangaraju, A. Panday, K.S. Raja, M. Misra, J. Phys. D Appl. Phys. 42 (2009) 135303.
[4] R. de Levie, Electrochim. Acta 8 (1963) 751.
[5] J.R. Park, D.D. Macdonald, Corros. Sci. 23 (1983) 295.
[6] C.M. Abreu, M. Izquierdo, P. Merino, X.R. Nóvoa, C. Pérez, Corrosion (NACE) 55 (1999) 1173.
[7] J.A. Nelder, R. Mead, Comput. J. 7 (1965) 308.
[8] F. Wang, R. Robert, N.A. Chernova, N. Pereira, F. Omenya, F. Badway, X. Hua, M. Ruotolo, R. Zhang, L. Wu, V. Volkov, D. Su, B. Key, M.S. Whittingham, C.P. Grey, G.G. Amatucci, Y. Zhu, J. Graetz, J. Am. Chem. Soc. 133 (2011) 18828.